Proceedings of ASME Turbo Expo 2008: Power for Land, Sea and Air
GT2008
June 9-13, 2008, Berlin, Germany

GT2008-51125

TRANSIENT COMBUSTION MODELING OF AN OSCILLATING LEAN PREMIXED METHANE/AIR FLAME

Jan A.M. Withag
Laboratory of Thermal Engineering
Department of
Mechanical Engineering
University of Twente
Enschede
The Netherlands
Email: j.a.m.withag@utwente.nl

Jim B.W. Kok*
Second Coauthor
Laboratory of Thermal Engineering
Department of
Mechanical Engineering
University of Twente
Enschede
The Netherlands
Email: j.b.w.kok@utwente.nl

Khawar Syed
Third Coauthor
Siemens Industrial
Turbomachinery Ltd.
PO Box 1,
Waterside South
Lincoln LN5 7FD, UK.

ABSTRACT

The main objective of the present study is to demonstrate accurate low frequency transient turbulent combustion modeling. For accurate flame dynamics some improvements were made to the standard TFC combustion model for lean premixed combustion. With use of a 1D laminar flamelet code, predictions have been made for the laminar flame speed and the critical strain rate to improve the TFC (Turbulent Flame Speed Closure) combustion model. The computational fluid dynamics program CFX is used to perform transient simulations. These results were compared with experimental data of Weigand et al [1]. Two different turbulence models have been used for predictions of the turbulent flow.

1 INTRODUCTION

In regular operation all gas turbine combustors have a significant combustion noise level induced by the turbulent fluctuation in the high power flame. This noise is characteristic for the operation as it is the result of the interaction between turbulence and combustion. Use is made of CFX 10 and its TFC model. The combustion model was improved by implementing highly accurate data for laminar flame speed and critical strain rate. The model is apllied and validated for a turbulent flame in a burner at atmospheric pressure and 30 kW. Description of the non-intrusive laser based optical measurements of this flame can be found in Weigand et al [1].

With the use of a 1-dimensional laminar flame code predictions have been made for the laminar flame speed and the critical strain rate in order to improve on the turbulent flame speed closure (TFC) combustion model. Two transient simulations were done with different turbulence models to optimize the predictions for the turbulent flow field. The transient simulations were time averaged and validated with time averaged measurement data. The experiments as done by Weigand et al [1] indicate that the case discussed here is an oscillating flame. The flame oscillates at a stable major frequency, with noise superimposed. In order to give an indication of the fluctuations in the combustor, several diagnostic variables are evaluated at multiple phase angles of the transient simulations.

2 TURBULENT FLAMESPEED CLOSURE (TFC) MODEL

The TFC model is based on the work of Zimont [2], but was only recently developed into a practical model, see Karpov et al [3, 4], Zimont and Lipatnikov [5], Zimont et al [6], and Zimont [7]. In its original form the model was only capable of modeling homogeneously premixed combustion. However in the

*Address all correspondence to this author.

last couple of years the model has been extended to partially premixed problems, Zimont et al [8], Biagioli et al [9], Zimont and Biagioli [10], and Polifke et al [11]. The TFC combustion model is specifically suitable for the ISP combustion regime [8], which is characteristic for industrial gas turbine combustors.

2.1 The basic TFC model

Like many other premixed combustion models, the TFC model employs the concept of a reaction progress variable. The progress variable, c, is a non-dimensional parameter that acts as a measure of the degree of 'completion of reaction' of the mixture, varying from zero in the unburnt mixture to one in the fully burnt mixture. It is defined either as a normalized temperature, or a normalized mass fraction:

$$c = \frac{T - T_r}{T_p - T_r} = \frac{Y_f - Y_{f,r}}{Y_{f,p} - Y_{f,r}} \tag{1}$$

where T is the temperature, Y_f is the fuel mass fraction, and the subscripts r and p refer to reactants and products respectively. It is possible to track the reaction through the domain by forming a transport equation for the Favre averaged progress variable for high Reynolds numbers:

$$\frac{\partial(\bar{\rho}\tilde{c})}{\partial t} + \nabla\cdot(\bar{\rho}\tilde{\mathbf{u}}\tilde{c}) = -\nabla\cdot(\overline{\rho\mathbf{u}''c''}) + \bar{\rho}\bar{\omega}. \tag{2}$$

In Eqn. (2) $\bar{\omega}$ is the progress variable source term and $\tilde{c}$ is the Favre averaged progress variable. The terms on the left hand side of Eqn. (2) can be computed directly, however, it is necessary to model those on the right for UraNS application. Important aspects in turbulent combustion modeling are the accurate representation of the diffusion term, the first term on the right hand side of Eqn. (2), and evaluation of a source term that depends realistically on both the chemical and turbulent processes.

The TFC model is different from other models based on a progress variable transport equation, by the source closure method used. Unlike other models where the diffusion and chemical source terms are modeled separately, the TFC model applies a joint closure. The gradient diffusion term is split into gradient and counter gradient components. The gradient diffusion is modeled by the standard approach, while the counter gradient transport is included in the closure for the chemical source term. The thus obtained closed reaction progress transport equation is:

$$\frac{\partial(\bar{\rho}\tilde{c})}{\partial t} + \nabla\cdot(\bar{\rho}\tilde{\mathbf{u}}\tilde{c}) = \nabla\cdot(\bar{\rho}D_t\nabla\tilde{c}) + \rho_u U_t|\nabla\tilde{c}| \tag{3}$$

where D_t is the turbulent diffusivity, ρ_u the unburnt density and U_t the turbulent flame speed. The significant advantage of this closure is that it allows the counter gradient transport to be incorporated without the use of higher order closures. Indeed it is not necessary to model the counter gradient transport at all, unless it is necessary to isolate it from the chemical source term. However, this also represents a drawback, as it is not possible to view the chemical source term unless the counter gradient transport is modeled. A more detailed discussion of the representation of counter gradient transport can be found in Zimont & Biagioli [10] and Zimont et al [8].

2.2 A model for the turbulent flame speed

It is clear from Eqn. (3) that in order to apply the TFC model, it is necessary to model the turbulent flame speed. Zimont has developed a correlation for the turbulent flame speed [2] in the thickened flamelet regime, according to this theory the unstrained turbulent flame speed is given by:

$$U_{t,unstr} = u_{n,t}\overline{\left(\frac{\partial S}{\partial S_0}\right)} \tag{4}$$

where $u_{n,t}$ is the propagation velocity of the thickened flamelet, ∂S is the area of a combustion front surface element, and ∂S_0 is the area of the projection of this element onto a plane perpendicular to the direction of flame propagation. It is then demonstrated that by modeling $u_{n,t}$ and $\overline{(\partial S/\partial S_0)}$ in Eqn. (4), and using relationships between the various flamelet properties it is possible to express the unstrained turbulent burning velocity as:

$$U_{t,unstr} = A\, u'^{3/4} S_{l,unstr}^{1/2} \chi^{-1/4} l_t^{1/4} \tag{5}$$

where A is a dimensionless constant, u' is the rms velocity fluctuation, $S_{l,unstr}$ the unstrained laminar flame speed, χ the thermal diffusivity, and l_t is the integral length scale. The value of A in Eqn. (5) has been shown, by Zimont & Lipatnikov [5], to be approximately 0.52 for a wide range of hydrocarbon fuels. The closure for the unstrained turbulent flame speed correlation needs the unstrained laminar flame speed as an input parameter. In this project the unstrained laminar flame speed was obtained using DIFFLA [1].

This closure for the turbulent flame speed does not account for effects of a large turbulent strain rate. A stretching factor G (Bray [12]) will be used to determine the strained turbulent flame speed:

$$U_t = G U_{t,unstr}. \tag{6}$$

A detailed description of the stretching factor is given in the next section.

[1] DIFFLA is a 1D laminar flame code developed at the university of Heidelberg

2.3 The modeling of flame stretch

Flame stretch is the combined effect of two turbulence-induced phenomena. The first is strain due to flow divergence, which can be interpreted as streamline curvature; and the second is strain due to a local velocity gradient. The effect of flame stretch is to reduce the residence time of the mixture, and thereby limit combustion.

The difficulty in modeling the effect of flame quenching is that the degree to which it occurs is dependent on the local turbulence. The model usually implemented with the TFC model is that due to Bray [12], based on the work of Liew et al [13] for non premixed combustion. It is assumed by Liew et al that only two local thermo chemical states exist and that the viscous dissipation rate, averaged over a characteristic volume is log-normally distributed. This allows the following expression to be written for the probability of finding a burning flamelet.

$$G = \frac{1}{2}\mathrm{erfc}\left[-\frac{1}{\sqrt{2\sigma}}\left(\ln\left(\frac{\varepsilon_{cr}}{\tilde{\varepsilon}}\right) - \frac{\sigma}{2}\right)\right] \tag{7}$$

where G is the stretch factor (the probability of finding a burning flamelet), erfc is the complementary error function, and ε_{cr} is the critical dissipation rate. The standard deviation of the log-normal distribution is represented by σ and is defined as:

$$\sigma^2 = \mu_{str} \ln \frac{l_t}{\eta} \tag{8}$$

where μ_{str} is a constant (usually 0.26), η is the Kolmogorov length scale, and l_t is the integral length scale. The stretch factor, G, then acts as a scaling factor for the chemical source term of the progress variable transport equation.

Several of the assumptions made by Liew et al [13] in developing Eqn. (7) are less suitable for premixed combustion. Implicit in the assumption that the progress variable and the degree of strain are statistically independent, is the assumption that the position of the flamelet does not depend on the strain. In the case of premixed combustion this is unlikely to be true, as is it possible for flamelets to move away from regions of high strain. To apply Eqn. (7) it is necessary to define a value for the critical dissipation rate, ε_{cr}. The following expression is suggested by Zimont et al [6]:

$$\varepsilon_{cr} = 15\nu g_{cr}^2 \tag{9}$$

where ν is the kinematic viscosity and g_{cr} is the critical velocity gradient for quenching. The difficulty is defining the critical velocity gradient. Although numerical calculations have been performed for simple cases, for example Rogg [14], it is less clear what the value would be in a gas turbine combustor. Good results were achieved by Polifke et al [11] for the flow in a gas turbine burner using the expression:

$$g_{cr} \propto \frac{S_l^2}{\chi} \qquad \text{where} \qquad \chi = \frac{k}{\rho c_p} \tag{10}$$

where S_l^2/χ is the inverse chemical time scale (τ_{ch}^{-1}). At elevated pressures this relationship broke down. In section 3.2 DIFFLA will be used in order to give a prediction of the critical velocity rate.

3 THE DIFFLA CODE

DIFFLA is a Fortran code developed by F. Behrendt and J. Warnatz of Heidelberg University in Germany. The DIFFLA code solves the governing equations for energy, mass fraction and momentum for non stationary laminar one-dimensional flames. It is therefore used to investigate the impact of different operating conditions or fuel composition upon laminar combustion behavior.

3.1 DIFFLA calculations to determine the unstrained laminar flame speed

An important input parameter for the TFC combustion model is the unstrained laminar flame speed $S_{l,unstr}$. With the use of DIFFLA it is possible to compute spatial profiles for the velocity in a one dimensional counter flowing flame. The extinction can clearly be identified by tracing the maximum temperature in the computational domain as strain increases. The actual extinction of the flame can be seen when the maximum temperature is the same as the preheat temperature. The strained laminar flame speed S_l is determined following Law et al [15]. Law et al use the the stretch K experienced by the flame in order to define the strained laminar flame speed. The flame stretch is defined as:

$$K = -\frac{du}{dx}. \tag{11}$$

The strained laminar flame speed of the stretched flame is defined to be the propagation velocity of the upstream boundary of the preheat zone. In this case S_l can be identified as the velocity at the point where K departs from linearity, The input parameter required for the TFC model is the unstrained laminar flame speed, i.e. the flame speed at zero strain rate. This is not a case that can be numerically simulated as this would mean that there would be a zero inlet velocity. For lower strain rates the plotted line in the laminar burning velocity against strain rate graph is almost linear. This behavior was found for all the equivalence ratios simulated. When assuming that the linear trend of the line

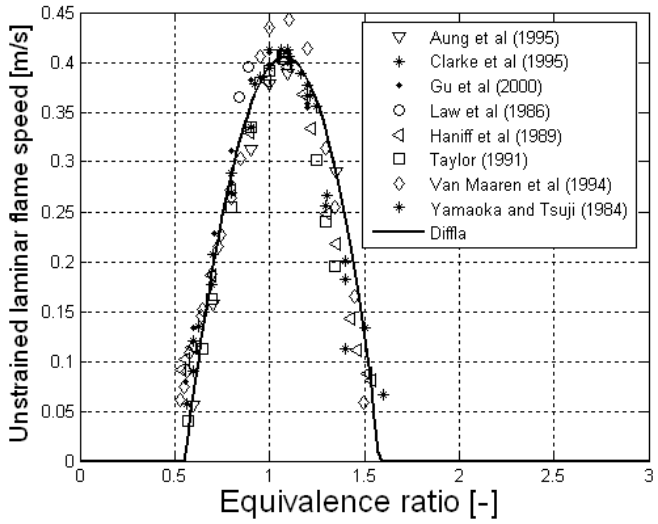

Figure 1. THE UNSTRAINED LAMINAR FLAME SPEED DERIVED WITH DIFFLA COMPARED WITH EXPERIMENTS. DESCRIPTION OF THE EXPERIMENTS CAN BE FOUND IN GU ET AL [16].

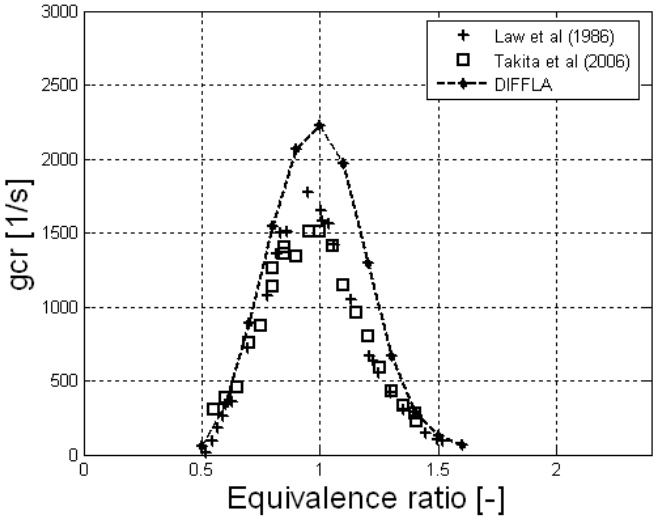

Figure 2. COMPARISON OF THE CRITICAL VELOCITY GRADIENT WITH EXPERIMENTAL DATA.

will continue to the case of zero strain we can determine the laminar flame speed for the case of zero strain rate, this assumption was also made in the experiment of Law [15].

Repeating this process for a set of equivalence ratios between 0.5 and 1.6 the solid line in Fig. 1 can be plotted. In this figure the unstrained laminar flame speed is plotted against equivalence ratio. This relation is implemented in CFX. Comparing DIFFLA's predictions of the unstrained laminar flame speed with experimental data Fig. 1, DIFFLA proves to be a good tool for predicting the laminar flame speed.

3.2 DIFFLA calculations to determine the critical velocity gradient

Zimont et al [6] have already commented that the critical velocity gradient for quenching g_{cr} cannot be determined directly from laminar flame calculations or asymptotic analysis. Instead, it was recommended to look upon g_{cr} as a tuning parameter, chosen for a given experiment and computation for a relevant set of validation cases. For this case DIFFLA is used to derive a correlation for the critical velocity gradient dependent on mixture fraction. For a given equivalence ratio ϕ, pressure p and preheat temperature T_u, a series of computations increasing strain were carried out until extinction occurred. In the case of the symmetrical fresh-to-fresh configuration, where opposing streams of fresh reactants flow towards a central reaction zone, extinction can clearly be identified by tracing the maximum temperature in the computational domain as strain increases. As the extinction strain rate is approached, the maximum temperature decreases very rapidly towards the preheat temperature. Repeating these steps for a series of equivalence ratios results in the points of extinction shown in Fig. 2.

4 TURBULENCE MODELING

CFX-10 provides with several different turbulence models ranging from the two-equation k−ε model to the Reynolds stress model with quadratic pressure strain-relation developed by Sarkar et al [17], the so called SSG model. In march of the year 2007 CFX-11 was released which enabled the users the use of a comparatively new approach to turbulence modelling. The so-called SAS model[2], by Menter and Egerov [18]. The SSG Reynolds stress model and the SST-SAS turbulence model were used in order to obtain results for the experiment as described by Weigand et al [1]. Both turbulence models will be described in this section.

4.1 The SSG Reynolds Stress Model.

In the SSG Reynolds stress model, a transport equation is solved for each component of the Reynolds stress tensor:

$$\frac{\partial \bar{\rho}\overline{\mathbf{u}''\mathbf{u}''}}{\partial t} + \nabla\cdot(\bar{\rho}\tilde{\mathbf{u}}\,\overline{\mathbf{u}''\mathbf{u}''}) = \nabla\cdot\left(\left(\mu + \frac{2}{3}c_s\rho\frac{\tilde{k}^2}{\tilde{\varepsilon}}\right)\nabla\overline{\mathbf{u}''\mathbf{u}''}\right) + \mathbf{P} + \Phi - \frac{2}{3}\bar{\rho}\tilde{\varepsilon}\delta, \tag{12}$$

the first term represents the transport by turbulent fluctuations, pressure fluctuations and viscous forces. **P** is the production

[2] Scale adaptive simulation model

Table 1. MODELING CONSTANTS FOR THE SSG REYNOLDS STRESS TURBULENCE MODEL.

$c_{\varepsilon 1} = 1.45$	$C_{s1} = 1.7$	$C_{\mu RS} = 0.1$	$C_{r1} = 0.9$
$c_{\varepsilon 2} = 1.83$	$C_{s2} = -1.05$	$s_{eRS} = 1.36$	$C_{r2} = 0.8$
		$c_s = 0.22$	$C_{r3} = 0.65$
			$C_{r4} = 0.625$
			$C_{r5} = 0.2$

term, Φ is the pressure-strain term which is the critical term for response to anisotropic behaviour and $\tilde{\varepsilon}$ is the dissipation rate. As the turbulence dissipation appears in the individual stress equations, an equation for $\tilde{\varepsilon}$ is required. This has the form:

$$\begin{aligned}\frac{\partial \bar{\rho}\tilde{\varepsilon}}{\partial t} + \nabla\cdot(\bar{\rho}\tilde{\mathbf{u}}\tilde{\varepsilon}) &= \frac{\tilde{\varepsilon}}{\tilde{k}}(c_{\varepsilon 1}P - c_{\varepsilon 2}\bar{\rho}\tilde{\varepsilon}) \\ &\quad + \nabla\cdot\left[\left(\mu + \frac{\mu_t}{\sigma_\varepsilon}\right)\nabla\tilde{\varepsilon}\right].\end{aligned} \tag{13}$$

The values of the constants for the SSG Reynolds Stress model are shown in Tab. 1.

4.2 The SST-SAS Turbulence Model

The Scale-Adaptive Simulation (SAS) is an extended URANS formulation, which allows the resolution of the turbulent spectrum in unstable flow conditions. The SAS concept is based on the introduction of the von Karman length scale in the turbulence scale equation. The information provided by the von Karman length scale allows SAS models to dynamically adjust to resolved structures in a URANS simulation, which results in an 'LES'-like behavior in unsteady regions of the flow field. At the same time, the model provides standard RANS capabilities in stable flow regions.

The starting point for the SST-SAS model is the the k-Φ formulation as given by Menter and Egorov [18]. The following two equations are derived for the variables k and $\Phi = \sqrt{k}L$:

$$\frac{\partial \bar{\rho}\tilde{k}}{\partial t} + \nabla\cdot(\bar{\rho}\tilde{\mathbf{u}}\tilde{k}) = P_k - c_\mu^{3/4}\bar{\rho}\frac{\tilde{k}^2}{\tilde{\Phi}} + \nabla\cdot\left(\frac{\nu_t}{\sigma_k}\nabla\tilde{k}\right) \tag{14}$$

$$\begin{aligned}\frac{\partial \bar{\rho}\tilde{\Phi}}{\partial t} + \nabla\cdot(\bar{\rho}\tilde{\mathbf{u}}\tilde{\Phi}) =& \zeta_1\frac{\tilde{\Phi}}{\tilde{k}}P_k - \zeta_2\nu_t S\left|U''\right|\frac{\tilde{\Phi}^2}{\tilde{k}^{3/2}} \\ &- \zeta_3\bar{\rho}\tilde{k} + \nabla\cdot\left[\frac{\nu_t}{\sigma_\Phi}\nabla\tilde{\Phi}\right]\end{aligned} \tag{15}$$

Table 2. MODELLING CONSTANTS FOR THE SST-SAS TURBULENCE MODEL.

$c_\mu = 0.09$	$\kappa = 0.41$	$\zeta_1 = 0.8$	$\sigma_k = 2/3$
		$\zeta_2 = 3.51$	$\sigma_\Phi = 2/3$
		$\zeta_3 = 0.0326$	

with:

$$P_k = \nu_t S^2, \quad \nu_t = c_\mu^{1/4}\tilde{\Phi} \quad \text{and} \quad \left|U''\right| = \left|\frac{\partial^2 U_i}{\partial x_j^2}\frac{\partial^2 U_i}{\partial x_j^2}\right|.$$

Where S is the absolute value of the strain rate, P_k is the production rate of the turbulent kinetic energy, the values for the constants used in Eqn. (14) and Eqn. (15) can be found in Tab. 2.

In order to provide the SAS capability to the SAS model, the Φ-equation is transformed to the $k-\omega$ framework using:

$$\tilde{\Phi} = \frac{1}{c_\mu^{1/4}}\frac{\tilde{k}}{\tilde{\omega}}. \tag{16}$$

The resulting ω-equation reads:

$$\begin{aligned}\frac{\partial \bar{\rho}\tilde{\omega}}{\partial t} + \nabla\cdot(\bar{\rho}\tilde{\mathbf{u}}\tilde{\omega}) =& \alpha\bar{\rho}S^2 - \beta\bar{\rho}\tilde{\omega}^2 + \nabla\cdot\left(\frac{\upsilon_t}{\sigma_\omega}\nabla\tilde{\omega}\right) \\ &+ \frac{2\bar{\rho}}{\sigma_\Phi}\left(\frac{1}{\tilde{\omega}}\nabla\cdot\left(\tilde{k}\nabla\tilde{\omega}\right)\right) \\ &+ F_{SST-SAS}.\end{aligned} \tag{17}$$

The first three terms of Eqn. (17) are the standard terms of the original Wilcox model [19]. The second term on the right hand side is the cross diffusion term, which would also result from the transformation of the k-ε to the k-ω model. It is also included in the SST model and helps to prevent the free stream sensitivity of the Wilcox model. The remaining term of the model is the $F_{SST-SAS}$ term. The main goal of this term is to preserve the SST model in the RANS regime and to activate the SAS capability in the URANS regions. The $F_{SST-SAS}$ is given by:

$$F_{SST-SAS} = -\frac{2\bar{\rho}}{\sigma_\Phi}\frac{\tilde{k}}{\tilde{\omega}}\left(\tilde{\omega}^2\nabla\cdot(\tilde{\omega}\nabla\tilde{\omega})\right) + \tilde{\zeta}_2\kappa\bar{\rho}S^2\frac{L}{L_{vK}} \tag{18}$$

In the RANS regime (and particularly in boundary layers) the two terms on the right hand side of Eqn. (18) are of the same

size, whereas the L_{vK} term dominates in the SAS regime:

$$\begin{array}{ll} \frac{2\tilde{\rho}}{\sigma_\Phi}\frac{\tilde{k}}{\tilde{\omega}^2}\left(\nabla\cdot(\tilde{\omega}\nabla\tilde{\omega})\right) \approx \tilde{\zeta}_2\kappa\bar{\rho}S^2\frac{L}{L_{vK}} & \text{(RANS regime)} \\ \frac{2\tilde{\rho}}{\sigma_\Phi}\frac{\tilde{k}}{\tilde{\omega}^2}\left(\nabla\cdot(\tilde{\omega}\nabla\tilde{\omega})\right) < \tilde{\zeta}_2\kappa\bar{\rho}S^2\frac{L}{L_{vK}} & \text{(SAS regime)} \end{array} \quad (19)$$

In order to preserve the SST model in the RANS region, the $F_{SST-SAS}$ term is modeled as follows:

$$F_{SST-SAS} = \bar{\rho}F_{SAS}\max\cdot \left[\tilde{\zeta}_2\kappa S^2\frac{L}{L_{vK}} - \frac{2}{\sigma_\Phi}\tilde{k}\max\left[\frac{\tilde{k}}{\tilde{\omega}^2}\left(\nabla\cdot(\tilde{\omega}\nabla\tilde{\omega})\right), \frac{1}{\tilde{k}^2}\nabla\cdot\left(\tilde{k}\nabla\tilde{k}\right)\right], 0\right]. \quad (20)$$

In Eqn. (20) the following constants are used:

$$F_{SAS} = 1.25, \qquad \tilde{\zeta}_2 = 1.755, \qquad \sigma_\Phi = 2/3.$$

5 SIMULATION OF THE COMBUSTION CHAMBER

The gas turbine model combustor was derived from an industrial design by Turbomeca. In Fig. 3 a schematic of the nozzle design with the combustion chamber is shown. Dry air at ambient temperature is fed via a plenum (diam. 78 mm) through the radial swirler vanes to the burner nozzle. The fuel gas (CH_4) is injected into the air flow through small holes within the radial swirler with high momentum to ensure good mixing before entering the combustion chamber. The air and fuel flow were each measured by two different mass flow meters.

The combustion chamber consists of large quartz windows of 1.5mm thickness held by steel posts thus creating a confinement of 85 mm x 85 mm and a height of $h = 144$ mm. The exit

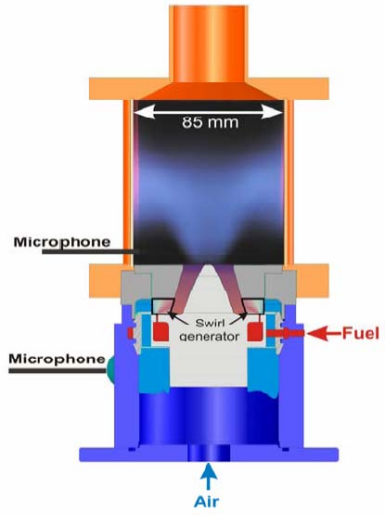

Figure 3. SCHEMATIC OF THE COMBUSTION CHAMBER USED IN WEIGAND ET AL [1].

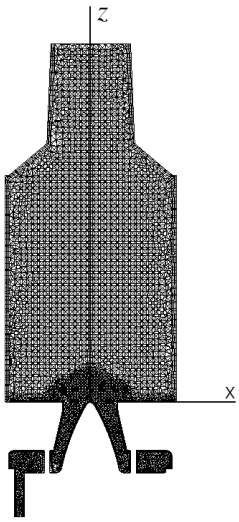

Figure 4. CROSS SECTION OF THE MESH USED FOR THE CFD SIMULATIONS.

of the upright combustion chamber is conically shaped leading to a short central exhaust pipe with a contraction ratio of approx. 0.2. The large windows on each side enable unobstructed optical access to nearly the whole flame zone, in particular close to the nozzle exit. In order to change the measuring location within the flames, the burner could be translated in axial and radial direction, and the position was measured by photo-electric encoder systems.

5.1 Computational domain

The computational domain is chosen to be the total domain of the combustion chamber used in Weigand et al [1]. An unstructured mesh of $6.56\cdot10^5$ tetrahedral elements, $2\cdot10^5$ wedges and 3000 pyramids was constructed. The region of the three air inlets, the swirler channels and the first part of the combustion chamber contain the smallest elements, with a grid size of 0.5 mm. In the combustion chamber the element size is enlarged toward grid sizes of 1 to 2 mm. Fig. 4 shows a cross section of the mesh, only one of the three air inlets is visible in this mesh. All transport equations are solved with a so-called high resolution discretization scheme. This scheme switches between the second order central differencing scheme and the first order upwind scheme depending on the local Courant number.

5.2 Inlet conditions

The boundary conditions were provided by Weigand et al [1] and related directly to the experimental points which they had considered. A summary of these conditions is given in Tab. 3. These boundary conditions were used to define the inlets for the CFX calculations.

Table 3. OPERATING CONDITIONS.

Air mass flow	732.6	[gram/min]
Fuel mass flow	35.7	[gram/min]
Equivalence ratio	0.84	[−]
Air inlet temperature	295	[K]
Fuel inlet temperature	295	[K]
Reference pressure	1	[bar]

6 ANALYSIS OF THE TIME AVERAGED RESULTS

Fig. 5 and Fig. 6 show the axial velocities along the x-axis at a height of $z = 5$mm and at a height of $z = 15$mm. A description of the x and z is shown in Fig. 4. As a result of the swirling flow, a central recirculation zone, necessary for flame stabilization is present. This recirculation zone can be identified by the negative axial velocities at the axis. The simulations with the SSG Reynolds stress and the SST-SAS turbulence model are compared with the measurements as done by Weigand et al [1]. Near the burner exit (Fig. 5) the Reynolds stress model clearly has difficulties predicting the magnitude of the inner recirculation zone and the maximum axial velocity. Further more downstream (Fig. 6) the Reynolds stress model gives a good prediction of the magnitude of the inner recirculation zone and the maximum axial velocity, but it fails to predict the right position for the peak of maximum axial velocity. The SAS model gives a good prediction of the location of the maximum axial velocity and the radial size of the recirculation zone.

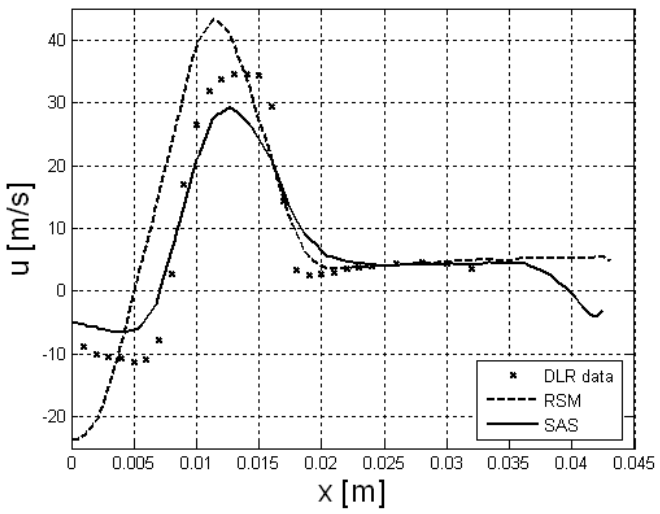

Figure 5. COMPARISON OF THE AXIAL VELOCITY PROFILE AT Z= 5MM.

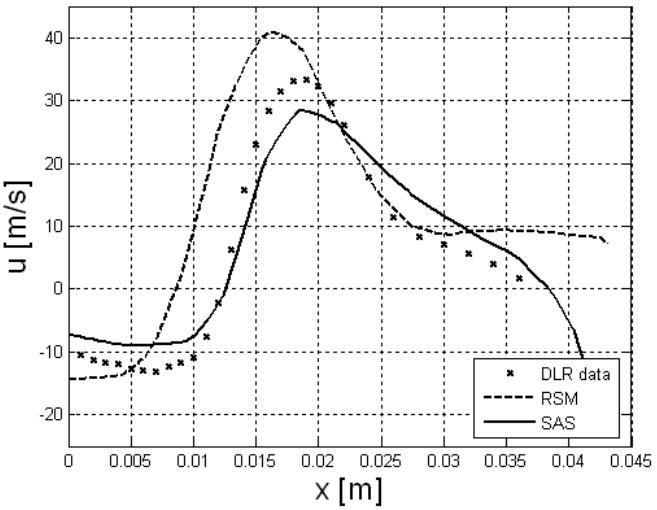

Figure 6. COMPARISON OF THE AXIAL VELOCITY PROFILE AT Z= 15MM.

Fig. 7 and Fig. 8 show the tangential velocities profiles along the x-axis. The swirling nature of the flow can be observed. The peak values decrease when moving further from the burner exit. Near the burner exit (Fig. 7) both simulations give a good prediction of the position of the maximum value of the tangential velocity. The prediction of the trend in the inner recirculation part of the flow is done best by the SST-SAS simulation. When focusing on the outer recirculation zones it is clear that both the

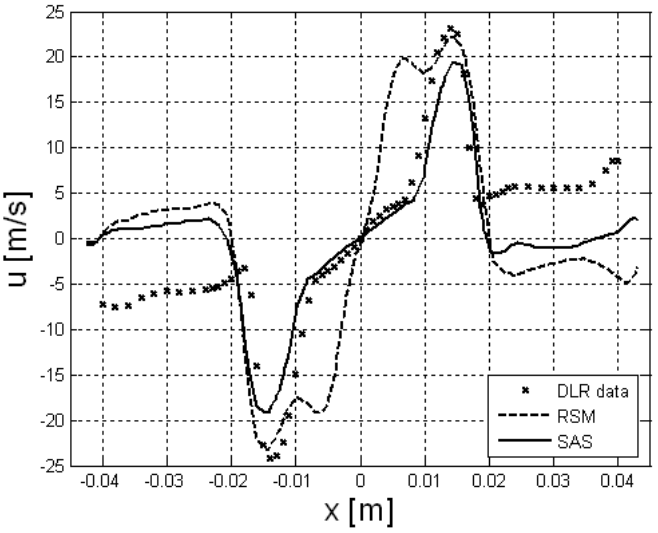

Figure 7. COMPARISON OF THE TANGENTIAL VELOCITY PROFILE AT $z = 5$mm.

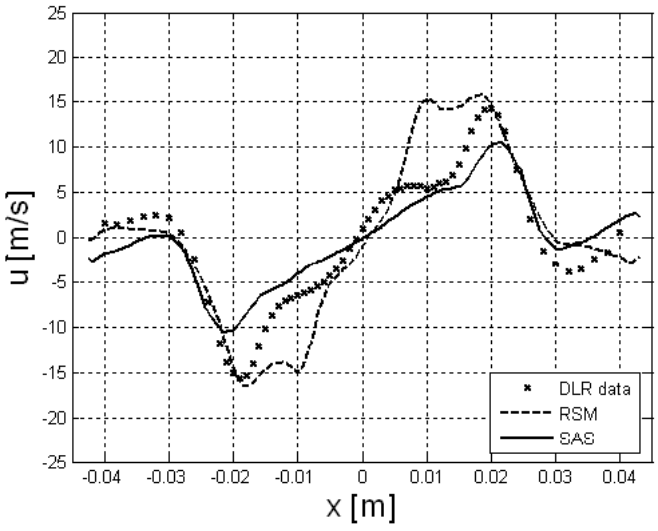

Figure 8. COMPARISON OF THE TANGENTIAL VELOCITY PROFILE AT $z = 15$mm.

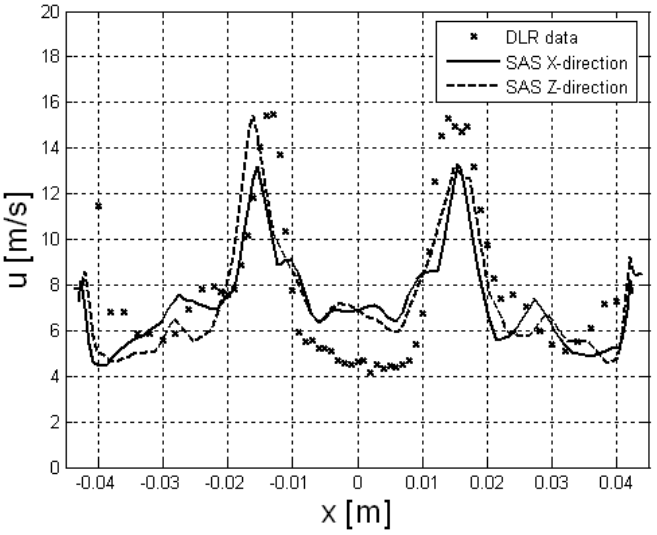

Figure 9. COMPARISON OF THE RMS OF THE AXIAL VELOCITY AT Z= 15MM.

simulations give a wrong prediction for the outer recirculation zone. Looking at Fig. 8 it can be seen that the SSG Reynolds stress simulation over predicts the maximum tangential velocity and gives the wrong position for the peak of maximum tangential velocity. The SST-SAS simulation performs not much better with a slight under prediction of the maximum tangential velocity and a good prediction for the position of the peak of maximum tangential velocity.

In Fig. 9 the axial Reynolds stress component is plotted against the x coordinate. Only a validation for the SST-SAS simulation is done with experimental data, as for the SSG Reynolds stress simulation no time average was derived for the Reynolds stress components. The peaks of the Reynolds stresses are caused by the shear layer of the inner recirculation zone and they show a reasonable resemblance with the experimental data.

Comparison between the temperatures measured in the experiments and the temperatures as predicted by the CFD simulations can be found in Fig. 10. The first thing important to mention is that in the CFD simulations the walls were assumed to be adiabatic. In the experiment the combustor walls were made of glass to provide visual access, which resulted in considerable heat loss through the walls. The result is an over prediction of the temperature near the wall. The position and value of the peak of maximum temperature is predicted very good in the simulations. The SSG Reynolds stress simulation fails to predict the magnitude of the minimum temperature and fails to predict the position of the minimum temperature in the part where the premixed gas/air flow enters the combustor chamber. The SST-SAS simulation gives a better prediction.

Fig. 11 shows the profile of the mixture fraction at a height of 15mm in the combustor chamber. The mixture fractions as predicted by both simulations are plotted against the data provided by Weigand et al [1]. In the inner recirculation part of the flow especially the SST-SAS simulation gives a good prediction of the mixture fraction. The SSG Reynolds stress simulation over predicts the maximum value of the mixture fraction in this part of the flow, and the SSG Reynolds stress simulation also gives a wrong prediction for the position of the peaks of maximum mixture fraction. In the outer recirculation part of the flow both

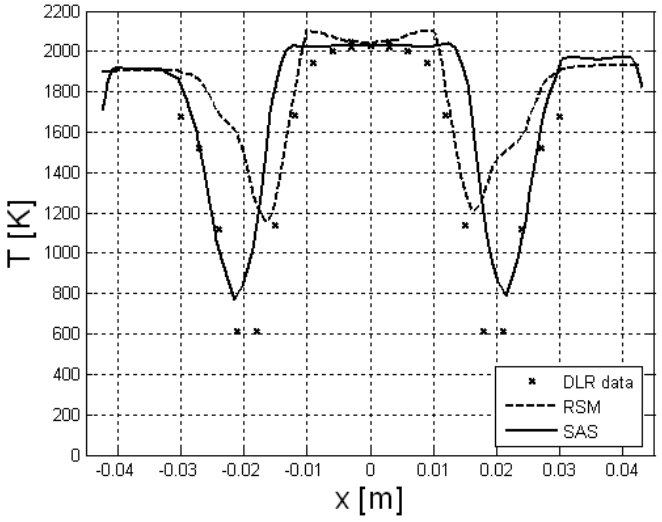

Figure 10. COMPARISON OF THE TEMPERATURE PROFILE AT Z= 15MM.

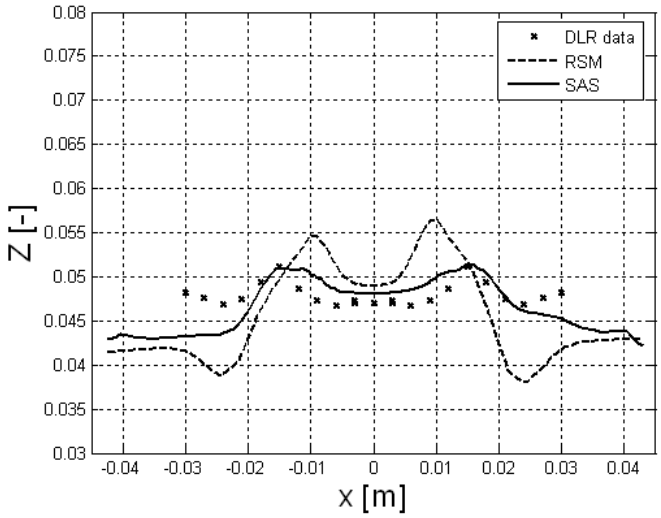

Figure 11. COMPARISON OF THE MIXTURE FRACTION PROFILE AT Z= 15MM.

simulations give a wrong prediction of the mixture fraction. This could well be explained by the weak outer recirculation zone predicted by the simulations for the tangential velocities in Fig. 8, the measured values clearly predict a stronger outer recirculation zone.

The time averaged results shown in this section show a reasonable comparison to the measured time averaged data as provided by Weigand et al [1]. These results should be handled with care as due to the very in stationary character of the flow compensating errors could influence the time averaged results. Compensating errors occur when different profiles result in the same time averaged profile. No time dependent results were available while writing this report, to compare the fluctuating values of the flow. At this moment the quality of the time averaged results with respect to compensating errors can not be assessed due to the absence of experimental data.

7 CONCLUSIONS

The Turbulent Flame speed Closure model for turbulent premixed combustion, as implemented in Ansys CFX v11, was improved by implementing highly accurate data for laminar flame speed and critical strain rate. The model was applied and validated on a turbulent flame in the burner used in Weigand et al [1] at atmospheric pressure and 30 kW. In the experiments the flame was observed to have an oscillating character. These combustion oscillations were also found in the Unsteady RaNS calculations performed with the improved TFC model and the SSG Reynolds stress and the SST-SAS turbulence models. The time averaged predicted radial profiles of axial and tangential velocity, rms of the axial velocity, temperature and mixture fraction, using the SST-SAS turbulence model, compare very well with the time averaged experimental data. The results obtained with the SSG-Reynolds stress turbulence model deviate significantly from the experimental data.

Hence the SST SAS turbulence model with the improved TFC combustion model proves to be a good choice for accurate turbulent combustion simulations.

ACKNOWLEDGMENT

The authors would like to thank CFX-ANSYS for the use of the code. The support of Siemens Industrial Turbomachinery Ltd UK to perform this research is highly appreciated.

REFERENCES

[1] Weigand, P., Meier, W., Duan, X., and Aigner, M., 2006. "Laser based investigations of thermoacoustic instabilities in a lean premixed gas turbine model combustor.". *Proceedings of ASME, (GT2006-90300)*.

[2] Zimont, V., 1979. "Theory of turbulent combustion of a homogeneous fuel mixture at high reynolds numbers". *Combustion, Explosion, and Shock Waves,* **15**(3), pp. 305–311.

[3] Karpov, V., Lipatnikov, A., and Zimont, V., 1994. "A model of premixed turbulent combustion and its validation". *Archivum Combustionis,* **14**(3), pp. 125–141.

[4] Karpov, V., Lipatnikov, A., and Zimont, V., 1996. "A test of an engineering model of premixed turbulent combustion". *Proc. Combust. Instit,* **26**, pp. 249–257.

[5] Zimont, V., and Lipatnikov, A., 1995. "A numerical model of premixed turbulent combustion of gases". *Chem. Phys. Reports,* **14**(7), pp. 993–1025.

[6] Zimont, V., Polifke, W., Bettelini, M., and Weisenstein, W., 1998. "An efficient computational model for premixed turbulent combustion at high reynolds numbers based on a turbulent flame speed closure". *Journal of engineering for gas turbines and power,* **120**(3), pp. 526–532.

[7] Zimont, V., 2000. "Gas premixed combustion at high turbulence. Turbulent flame closure combustion model". *Experimental Thermal and Fluid Science,* **21**(1-3), pp. 179–186.

[8] Zimont, V., Biagioli, F., and Syed, K., 2001. "Modelling turbulent premixed combustion in the intermediate steady propagation regime". *Progress in Computational Fluid Dynamics, An International Journal,* **1**(1/2/3), pp. 14–28.

[9] Biagioli, F., Zimont, V., and Syed, K., 2001. "Modelling and numerical simulation of gas combustion in DLE burners based on a turbulent flame speed closure approach". *The 2001 International Joint Power Generation Conference & Exposition, New Orleans, Louisiana, USA. June 4-7.*

[10] Zimont, V., and Biagioli, F., 2002. "Gradient, countergradient transport and their transition in turbulent premixed

flames". *Combustion Theory and Modelling,* **6**(1), pp. 79–101.

[11] Polifke, W., Flohr, P., and Brandt, M., 2002. "Modelling of Inhomogeneously Premixed Combustion With an Extended TFC Model". *Journal of Engineering for Gas Turbines and Power,* **124**, p. 58.

[12] Bray, K., 1986. "Methods of including realistic chemical reaction mechanisms in turbulent combustion models". *Proceedings of the Second Workshop on The Modelling of Chemical Reaction Systems, Heidelberg, Germany*, pp. 356–375.

[13] Liew, S., Bray, K., and Moss, J., 1984. "Stretched laminar flamelet model of turbulent nonpremixed combustion". *Combustion and Flame,* **56**, pp. 199–213.

[14] Rogg, B., 1988. "Response and flamelet structure of stretched premixed methane-air flames". *Combust. Flame,* **73**, pp. 45–46.

[15] Law, C., Zhu, D., and Yu, G., 1988. "Propagation and extinction of stretched premixed flames". *Symposium(International) on Combustion, 21 st, Munich, Federal Republic of Germany*, p. 1988.

[16] Gu, X., Haq, M., Lawes, M., and Woolley, R., 2000. "Laminar burning velocity and Markstein lengths of methane-air mixtures". *Combustion and Flame,* **121**(1-2), pp. 41–58.

[17] Speziale, C., Sarkar, S., and Gatski, T., 2006. "Modelling the pressure–strain correlation of turbulence: an invariant dynamical systems approach". *Journal of Fluid Mechanics Digital Archive,* **227**, pp. 245–272.

[18] Menter, F., and Egorov, Y. "Revisiting the turbulent scale equation". *Proceedings of the IUTAM Symposium" One Hundred Years of Boundary Layer Research" held in Gottingen,(12-14 August 2004)*.

[19] Wilcox, D. *Turbulence Modeling for CFD*. DCW Industries, Inc., La Cañada.